# Upright Pyramid Surface Textures for Light Trapping and MoOx Layer in Ultrathin Crystalline Silicon Solar Cells

Halo D. Omar

Department of Physics, Faculty of Science and Health, Koya University,
Koya KOY45, Kurdistan Region - F.R. Iraq

***Abstract*—In this work, ray tracing is used to investigate the optical characteristics of various surface structures in ultrathin crystalline silicon (c-Si) for solar cells. Ultrathin c-Si with a thickness of 20 μm is used as the substrate. The light trapping includes front upright pyramids with a molybdenum oxides (MoOx) anti-reflection (AR) layer. Planar ultrathin c-Si (without a MoOx AR layer and upright pyramids) is used as a reference. The wafer ray tracer was developed by a photovoltaic (PV) lighthouse to model the MoOx AR layer to reduce the front surface reflectance and impacts of the AR layer on ultrathin Si solar cells. The optical properties are calculated on the AM1.5 global solar energy spectrum across the 200–1200 nm wavelength region. From the absorbance profile, the photogenerated current density ($J_{ph}$) in the substrate is also calculated with various surface structures. The front upright pyramids with the MoOx layer result in the largest absorbance enhancement due to the enhanced light scattering by the pyramids and MoOx AR layer. The $J_{ph}$ of 37.41 mA/cm² is improved when compared to the planar ultrathin c-Si reference. This study is significant as it illustrates the potential of ultrathin c-Si as a promising PV module technology in the future.**

***Index Terms*—Absorbance, Crystalline silicon, Light trapping, MoOx, Solar Cells**

## I. Introduction

Crystalline silicon (c-Si) solar cells have been dominating the photovoltaic (PV) market for more than 90% of the PV market share due to the high efficiency of c-Si, a non-toxic material, potentially lower manufacturing costs, and being naturally abundant on the earth crust (Zhou, et al., 2024). Today, 180 μm-thick c-Si is usually used for solar cell production (Li, et al., 2024). Reducing the c-Si thickness is an attractive solution to reduce the fabrication cost of the solar cells (Xue, et al., 2020). However, ultrathin c-Si solar cells suffer poor photogenerated current density ($J_{ph}$) due to their reduced absorbance at long wavelengths of light (Huang, et al., 2024, Li, et al., 2024). Light trapping strategies, such as microtextured surfaces and anti-reflection (AR) layers, have been commonly studied to increase effective light absorbance and reduce surface reflectance losses (Kanda, et al., 2016; Macco, 2015). In the literature, various materials have been used as AR layers on c-Si solar cells, such as silicon nitride (SiNx), aluminum oxide ($Al_2O_3$), silicon dioxide ($SiO_2$) magnesium fluoride ($MgF_2$), titanium dioxide ($TiO_2$), and zinc oxide (ZnO) (Shanmugam, et al., 2020, Zin, et al., 2018). This study aims to evaluate the MoOx AR layer with various surface structures in the ultrathin c-Si solar cells to observe several optical effects. The AR layer, such as ZnO and $SiO_2/Si_3N_4$, is used on the front c-Si surface (Chee, et al., 2018). By coating the Si surface with various thicknesses of AR layers of ZnO and $SiO_2/Si_3N_4$, the average reflectance shows about zero at the wavelength of 525 nm. Without the AR layer, the Si substrate achieves an average reflectance of about 40% at the same wavelength. The AR layer cells give a 1.15% efficiency improvement on Si when compared to the solar cells without the AR layer. In addition, the surface texture of a c-Si solar cell with an AR layer shows a conversion of 15.5% when compared to the surface texture of a c-Si solar cell without an AR layer (efficiency of 13.8%), due to the lower reflectance and improved light absorbance in the c-Si solar cell (Kanda, et al., 2016). However, the incident photon into the ultrathin c-Si is grading effect by the refractive index (n) within the molybdenum oxides (MoOx, n = 2) AR layer that is enclosed between air (n = 1) and ultrathin c-Si (n = 3.94 at 600 nm) (Macco, 2015, Lu, et al., 2018). Besides, microscale random upright pyramids have a suitable geometry for ultrathin c-Si with a thickness of 20 μm. Due to the enhanced scattering of incident light by pyramids at oblique angles, it leads to enhanced light absorbance in the ultrathin c-Si cells since the dimensions of the random pyramids are larger than the wavelength of the light (Garín, et al., 2023). In the conventional strategy used for industrial c-Si, solar cells are combined with an AR layer and upright pyramids to minimize surface reflectance losses on the front surface (Valiei, et al., 2022, Tahir, et al., 2024). Omar et al. have also studied the thin

ARO-The Scientific Journal of Koya University
Vol. XII, No. 1 (2024), Article ID: ARO. 11586. 4 pages
Doi: 10.14500/aro.11586
Received: 27 March 2024; Accepted: 05 June 2024
Regular research paper: Published: 25 June 2024
Corresponding author's e-mail: halo.dalshad@koyauniversity.org

http://dx.doi.org/10.14500/aro.11586

c-Si solar cell with different light-trapping schemes by ray tracing simulation. The highest $J_{ph}$ of 39.1 mA/cm$^2$ is calculated by the SiNx layer on the inverted pyramids presented by (Omar Hashim and Pakhuruddin, 2020).

This study utilizes ray tracing simulation to investigate various surface structures in ultrathin c-Si cells. Ultrathin c-Si with a thickness of 20 µm is used to simulate the performance of upright pyramids for light trapping in c-Si. Ray tracing is used to investigate the MoOx AR layer and the light-trapping performance of upright pyramids in ultrathin c-Si for application in solar cells. Wafer ray tracing simulation studies the transmittance, reflectance, and absorbance of each substrate over a wavelength range of 200 nm to 1200 nm. The photogenerated current density ($J_{ph}$) can be calculated from the absorbance result. Planar ultrathin c-Si (without a MoOx layer and upright pyramids) is shown as a reference.

## II. Methodology

PV Lighthouse is used with Wafer Ray Tracer software for light trapping in ultrathin c-Si with 20 µm thickness. The angle of the incidence is at zero degrees, and the AM 1.5 global solar spectrum is selected across the 200–1200 nm wavelength region (with an interval of 10 nm). The ray tracing uses a maximum total ray of 50,000 with 5,000 numbers of rays per run. The optical properties of ultrathin c-Si with different surface structures are designed with a front random upright pyramid (texture angle of 54.7°, width of 5.6 µm, and height of 4 µm) and 75 nm MoOx as AR layer (by atomic layer deposition ALD) as considered to cover the 200–1200 nm spectral region. Fig. 1 illustrates cross-sectional schematic diagrams of ultrathin c-Si with 20-µm thickness and various surface structures. Fig. 1a illustrates planar ultrathin c-Si, which is used as a reference. The planar ultrathin c-Si does not have a front MoOx AR layer or upright pyramids on either surface. Fig. 1b shows the front MoOx AR layer on planar ultrathin c-Si. Fig. 1c and d demonstrates two light traps with and without the front MoOx AR layer.

The potential photogenerated current density ($J_{ph}$) is calculated by integrating the absorbance result; EQE is the external quantum efficiency (EQE = IQE x A) of the cell; q is the elementary charge; and the solar spectrum S(λ) is calculated from the AM1.5 global solar energy spectrum across the 200–1200 nm wavelength region (Pakhuruddin, 2020; Pakhuruddin, et al., 2016). In equation (1), the carrier collection is assumed to be one (i.e., internal quantum efficiency, IQE = 1).

$$J_{ph} = q\int EQE(\lambda).S(\lambda)d\lambda \quad \text{(I)}$$

## III. Results and Discussion

Reflectance, transmittance, and absorbance profiles of four surface types are depicted in Fig. 2. The planar ultrathin c-Si (without MoOx and pyramids) measures a surface reflection of about 0.35 for incident light at a wavelength of 600 nm and decreases to around zero after the 75 nm MoOx AR layer (Hu, et al., 2022). The reflectance appears from the difference in the refractive index of air (n = 1) and c-Si (n = 3.94 at 600 nm) (Macco, 2015; Lu, et al., 2018). The transmittance is about 0.5 at a wavelength of 1200 nm. The transmittance loss is high because of the low thickness of the ultrathin c-Si absorber. The planar ultrathin c-Si shows weak light absorbance across the 200–1200 nm wavelength region. The MoOx AR layer on planar ultrathin c-Si leads to reduced surface reflectance from the ultrathin c-Si. As a result, the surface reflectance improves significantly. The front pyramid illustrates a reflectance of 0.1 at the 600 nm wavelength. By using the MoOx layer on randomly upright pyramids with an ultrathin c-Si surface, the reflectance is decreased significantly to a minimum of 0.03 at wavelength regions between 450 and 850 nm. The light absorbance increases up to 0.95 at the same wavelength. As a result, the transmittance drops to 0.3 due to the enhanced scattering at the surface of the ultrathin c-Si. The transmittance values of the planar and MoOx AR layers on the planar surface are 0.5 and 0.6, respectively, above the 1100 nm region. A transmittance spectrum does not change with the MoOx layer on pyramids or without the AR layer on pyramids (OmarHashim and Pakhuruddin, 2020).

Table I depicts the resulting $J_{ph}$ of ultrathin c-Si with various surface structures. Planar ultrathin c-Si is also included as a reference. Planar ultrathin c-Si demonstrates a $J_{ph}$ of 21.12 mA/cm$^2$. For a MoOx layer on planar ultrathin c-Si, the calculated $J_{ph}$ is about 29.57 mA/cm$^2$, due to the improved light coupling into the ultrathin c-Si absorber. With front upright pyramids on ultrathin c-Si, the $J_{ph}$ is increased to 35.26 mA/cm$^2$. In addition, using 75 nm MoOx on upright pyramids, the $J_{ph}$ is increased to 37.41 mA/cm$^2$ compared to the ultrathin c-Si with pyramids (with AR effect). This leads to increased light absorbance, as illustrated in Fig. 2c.

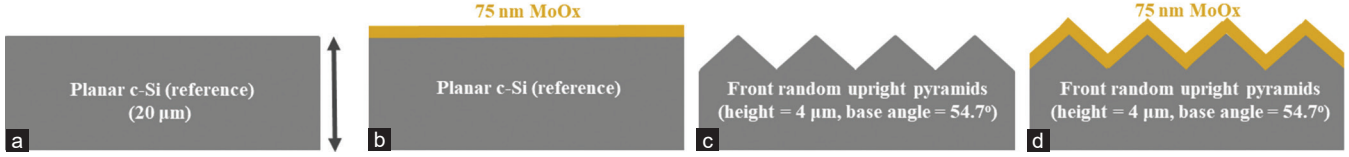


Fig. 1. Schematic diagram of ultrathin crystalline silicon (c-Si) (with 20 µm thickness) substrate (a) Planar ultrathin c-Si (without MoOx and upright pyramids) (b) MoOx AR layer on planar ultrathin c-Si; (c) front random upright pyramids (without MoOx) (d) front random upright pyramids with a front MoOx AR layer. The drawings are not to scale.

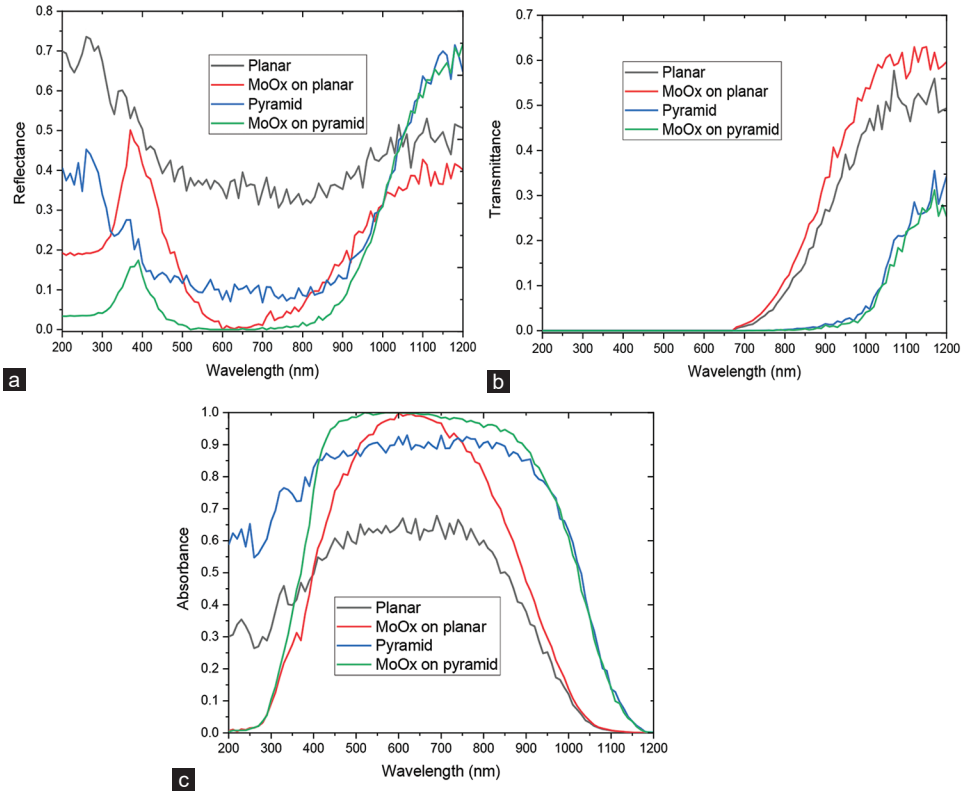


**Fig. 2.** (a-c) The light reflectance, transmittance, and absorbance spectra of the ultrathin crystalline silicon (c-Si) with various surface structures. Planar ultrathin c-Si (without MoOx layer and upright pyramids) is shown as a reference.

TABLE I
THE POTENTIAL $J_{PH}$ OF ULTRATHIN C-SI WITH VARIOUS SURFACE STRUCTURES, AS DEPICTED IN FIG. 1. PLANAR ULTRATHIN C-SI IS USED AS A REFERENCE

| Surface structures | $J_{ph}$ (mA/cm$^2$) |
|---|---|
| Planar | 21.12 |
| MoOx on planar | 29.57 |
| Front pyramid | 35.26 |
| MoOx on pyramid | 37.41 |

c-si: Crystalline silicon, $J_{ph}$: Photogenerated current density

## IV. CONCLUSION

This study utilizes ray tracing simulation to investigate various surface structures in ultrathin c-Si cells. Ultrathin c-Si with a thickness of 20 μm is used as a substrate. The optical characteristics of ultrathin c-Si with different surface structures (with or without a 75 nm MoOx layer and randomly upright pyramids) are measured across the spectral region of 200–1200 nm. Planar ultrathin c-Si (without MoOx and upright pyramids) is used as a reference. The reflectance of ultrathin c-Si is about 0.35 at a wavelength of 600 nm. In the MoOx layer on ultrathin c-Si, the front surface reflectance reduces to zero at a wavelength of 600 nm due to its low refractive index (MoOx, n = 2 at 600 nm). With front upright pyramids, the reflectance drops to 0.1 at the same wavelength due to the enhanced scattering at the surface of the ultrathin c-Si. Using the MoOx layer on randomly upright pyramids with an ultrathin c-Si surface, lower reflectance and the highest $J_{ph}$ of 37.41 mA/cm$^2$ are achieved.

## REFERENCES

Chee, K.W.A., Tang, Z., Lü, H., and Huang, F., 2018. Anti-reflective structures for photovoltaics: Numerical and experimental design. *Energy Reports*, 4, 266-273.

Garín, M., Pasanen, T.P., López, G., Vähänissi, V., Chen, K., Martín, I., and Savin, H., 2023. Black ultra-thin crystalline silicon wafers reach the $4n^2$ absorption limit-application to IBC solar cells. *Small*, 19, 2302250.

Hu, Q., Wang, J., Lu, Y., Tan, R., Li, J., and Song, W., 2022. Sputtering-deposited thin films on textiles for solar and heat managements: A mini-review. *Physica Status Solidi (a)*, 219, 2100572.

Huang, S., Xu, C., Wang, G., Du, J., Yu, J., Zhang, L., Meng, F., Zhao, D., Li, R., Huang, H., Liu, Z., and Liu, W., 2024. Smaller texture improves flexibility of crystalline silicon solar cells. *Materials Letters,* 357, 135768.

Kanda, H., Uzum, A., Harano, N., Yoshinaga, S., Ishikawa, Y., Uraoka, Y., Fukui, H., Harada, T., and Ito, S., 2016. $Al_2O_3/TiO_2$ double layer anti-reflection coating film for crystalline silicon solar cells formed by spray pyrolysis. *Energy Science and Engineering*, 4, 269-276.

Li, Y., Ru, X., Yang, M., Zheng, Y., Yin, S., Hong, C., Peng, F., Qu, M., Xue, C., Lu, J., Fang, L., Su, C., Chen, D., Xu, J., Yan, C., Li, Z., Xu, X., and Shao, Z., 2024. Flexible silicon solar cells with high power-to-weight ratios. *Nature*, 626, 105-110.

Lu, C., Rusli, Prakoso, A.B., and Li, Z., (2018). Aqueous Solution Deposited Molybdenum oxide Crystalline Silicon Heterojunction Solar Cells. In: *2018 IEEE 7th World Conference on Photovoltaic Energy Conversion (WCPEC) (A Joint Conference of 45th IEEE PVSC, 28th PVSEC and 34th EU PVSEC)*, pp.2155-2157.

Macco, B., Vos, M., Thissen, N.F.W., Bol, A.A., and Kessels, W.M.M., 2015. Low-temperature atomic layer deposition of MoOx for silicon heterojunction solar cells. *Physica Status Solidi*, 9, 393-396.

Omar, H.D., Hashim, M.R., and Pakhuruddin, M.Z., 2020. Ray tracing of

inverted pyramids for light-trapping in thin crystalline silicon for solar cells. *Optik*, 219, 165279.

Pakhuruddin, M.Z., 2020. *Ray tracing of light trapping schemes in thin crystalline silicon for photovoltaics. Solid State Phenomena*. Trans Tech Publications, Switzerland, pp.183-191.

Pakhuruddin, M.Z., Huang, J., Dore, J., and Varlamov, S., 2016. Enhanced absorption in laser-crystallized silicon thin films on textured glass. *IEEE Journal of Photovoltaics,* 6, 852-859.

Shanmugam, N., Pugazhendhi, R., Madurai Elavarasan, R., Kasiviswanathan, P., and Das, N., 2020. Anti-reflective coating materials: A holistic review from PV perspective. *Energies*, 13, 2631.

Tahir, S., Saeed, R., Ashfaq, A., Ali, A., Mehmood, K., Almousa, N., Shokralla, E.A., Macadangdang, R.R. Jr., Soeriyadi, A.H., and Bonilla, R.S., 2024. Optical modeling and characterization of bifacial SiNx/AlOx dielectric layers for surface passivation and antireflection in PERC. *Progress in Photovoltaics: Research and Applications,* 32, 63-72.

Valiei, M., Shaibani, P.M., Abdizadeh, H., Kolahdouz, M., Asl Soleimani, E., and Poursafar, J., 2022. Design and optimization of single, double and multilayer anti-reflection coatings on planar and textured surface of silicon solar cells. *Materials Today Communications*, 32, 104144.

Xue, M., Nazif, K.N., Lyu, Z., Jiang, J., Lu, C.Y., Lee, N., Zang, K., Chen, Y., Zheng, T., Kamins, T.I., Brongersma, M.L., Saraswat, K.C., and Harris, J.S., 2020. Free-standing 2.7 μm thick ultrathin crystalline silicon solar cell with efficiency above 12.0%. *Nano Energy*, 70, 104466.

Zhou, Y., Wen, J., Zheng, Y., Yang, W., Zhang, Y., and Cheng, W., 2024. Status quo on recycling of waste crystalline silicon for photovoltaic modules and its implications for China's photovoltaic industry. *Frontiers in Energy*.

Zin, N., Mcintosh, K., Bakhshi, S., Vázquez-Guardado, A., Kho, T., Fong, K., Stocks, M., Franklin, E., and Blakers, A., 2018. Polyimide for silicon solar cells with double-sided textured pyramids. *Solar Energy Materials and Solar Cells,* 183*,* 200-204.